CrossMark

Galaxy and Quasar Fueling Caught in the Act from the Intragroup to the Interstellar Medium

Sean D. Johnson[1,2,11] , Hsiao-Wen Chen[3] , Lorrie A. Straka[4] , Joop Schaye[4] , Sebastiano Cantalupo[5], Martin Wendt[6,7],
Sowgat Muzahid[4] , Nicolas Bouché[8] , Edmund Christian Herenz[9], Wolfram Kollatschny[10], John S. Mulchaey[2],
Raffaella A. Marino[5] , Michael V. Maseda[4] , and Lutz Wisotzki[6]

[1] Department of Astrophysical Sciences, 4 Ivy Lane, Princeton University, Princeton, NJ 08544, USA; sdj@astro.princeton.edu
[2] The Observatories of the Carnegie Institution for Science, 813 Santa Barbara Street, Pasadena, CA 91101, USA
[3] Department of Astronomy & Astrophysics, The University of Chicago, 5640 South Ellis Avenue, Chicago, IL 60637, USA
[4] Leiden Observatory, Leiden University, P.O. Box 9513, NL-2300 RA Leiden, The Netherlands
[5] Department of Physics, ETH Zurich, Wolfgang-Pauli-Strasse 27, 8093, Zurich, Switzerland
[6] Leibniz-Institut für Astrophysik Potsdam (AIP), An der Sternwarte 16, D-14482 Potsdam, Germany
[7] Institut für Physik und Astronomie, Universität Potsdam, Karl-Liebknecht-Str. 24/25, D-14476 Golm, Germany
[8] Univ Lyon, Univ Lyon1, Ens de Lyon, CNRS, Centre de Recherche Astrophysique de Lyon UMR5574, F-69230, Saint-Genis-Laval, France
[9] Department of Astronomy, Stockholm University, AlbaNova University Centre, SE-106 91 Stockholm, Sweden
[10] Institut für Astrophysik, Universität Göttingen, Friedrich-Hund Platz 1, D-37077 Göttingen, Germany

Abstract

We report the discovery of six spatially extended (10–100 kpc) line-emitting nebulae in the $z \approx 0.57$ galaxy group hosting PKS 0405−123, one of the most luminous quasars at $z < 1$. The discovery is enabled by the Multi Unit Spectroscopic Explorer and provides tantalizing evidence connecting large-scale gas streams with nuclear activity on scales of <10 proper kpc (pkpc). One of the nebulae exhibits a narrow, filamentary morphology extending over 50 pkpc toward the quasar with narrow internal velocity dispersion ($50 \, \mathrm{km \, s^{-1}}$) and is not associated with any detected galaxies, consistent with a cool intragroup medium filament. Two of the nebulae are 10 pkpc north and south of the quasar with tidal-arm–like morphologies. These two nebulae, along with a continuum-emitting arm extending 60 pkpc from the quasar, are signatures of interactions that are expected to redistribute angular momentum in the host interstellar medium (ISM) to facilitate star formation and quasar fueling in the nucleus. The three remaining nebulae are among the largest and most luminous [O III] emitting "blobs" known (1400–$2400 \, \mathrm{pkpc^2}$) and correspond both kinematically and morphologically to interacting galaxy pairs in the quasar host group, consistent with arising from stripped ISM rather than large-scale quasar outflows. The presence of these large- and small-scale nebulae in the vicinity of a luminous quasar bears significantly on the effect of large-scale environment on galaxy and black hole fueling, providing a natural explanation for the previously known correlation between quasar luminosity and cool circumgalactic medium.

Key words: galaxies: interactions – intergalactic medium – quasars: general – quasars: individual (PKS 0405–123)

1. Introduction

Galaxy−galaxy interactions represent one of the few cosmologically viable mechanisms for redistributing angular momentum in the interstellar medium (ISM) to fuel luminous quasars and nuclear star formation (Hopkins & Hernquist 2009, and references therein). In cosmological simulations of galaxy evolution, mergers play a significant role in fueling black hole growth at $z < 1$ (e.g., McAlpine et al. 2018). Despite these expectations and over 50 years of observations, the importance of interactions in fueling quasars is still debated, with studies finding evidence both against (e.g., Villforth et al. 2014) and in favor (e.g., Goulding et al. 2018) of interactions as a major triggering mechanism.

Insights into quasar fueling can be gained through observations of gas in quasar host environments. Observations through H I 21 cm emission are largely limited to the local Universe, while quasar activity peaked at $z \approx 2$ (e.g., Schmidt et al. 1995) leaving few available targets. More sensitive surveys using background absorption spectroscopy reveal the common presence of cool ($\approx 10^4 \, \mathrm{K}$) circumgalactic medium (CGM) in quasar host halos (Bowen et al. 2006; Hennawi et al. 2006;

Prochaska et al. 2013; Farina et al. 2014; Johnson et al. 2015) at projected distances of $d \lesssim 300 \, \mathrm{pkpc}$. This cool CGM exhibits extreme kinematics and is strongly correlated with quasar luminosity, suggesting a physical connection between quasar activity and the CGM at $z \approx 1$ (for a study of the CGM of low-luminosity active galactic nuclei (AGN), see Berg et al. 2018).

The lack of morphological information in absorption-line surveys makes it difficult to differentiate between cool CGM often observed around massive galaxies (e.g., Chen et al. 2018), debris from interactions thought to fuel nuclear activity (e.g., Villar-Martín et al. 2010), and outflows (e.g., Greene et al. 2012). Even when morphologies of extended nebulae around quasars are available from imaging (e.g., Stockton & MacKenty 1987; Sun et al. 2017) or narrow-field integral field spectrographs (IFSs; e.g., Fu & Stockton 2009; Liu et al. 2013; Husemann et al. 2013), discerning the origins of the nebulae can be difficult. Nevertheless, such emitting "blobs" are often attributed to outflows (e.g., Fu & Stockton 2009; Schirmer et al. 2016; Yuma et al. 2017).

New wide-field IFSs such as the Multi Unit Spectroscopic Explorer (MUSE; Bacon et al. 2010) provide a powerful means of simultaneously surveying the galactic and gaseous environments of quasars, allowing both sensitive searches for extended, ionized nebulae and joint studies of their morphologies and

---

kinematics in the context of neighboring galaxies. MUSE already enabled the discovery of extended nebulae around AGN in the field (Powell et al. 2018), in group or cluster environments (Poggianti et al. 2017; Epinat et al. 2018), and around luminous quasars at $z \approx 3$ (e.g., Borisova et al. 2016).

Here, we present the discovery of ionized nebulae on scales of 10–100 pkpc in the environment of PKS 0405−123, one of the most luminous quasars in the $z < 1$ Universe.[12] Joint analyses of the nebular morphologies and kinematics indicate that they arise from cool filaments and interaction-related debris, rather than outflows. These observations provide novel insights into galaxy and quasar fueling from intragroup medium (IGrM) to ISM scales.

This Letter proceeds as follows. In Section 2 we describe the MUSE observations and analysis. In Section 3, we present the galactic environment of PKS 0405−123. In Section 4, we present the discovery of multiple extended nebulae around the quasar and discuss their origins. In Section 5 we consider the implications of our findings.

Throughout, we adopt a flat Λ cosmology with $\Omega_m = 0.3$, $\Omega_\Lambda = 0.7$, and $H_0 = 70$ km s^{-1} Mpc^{-1}.

2. Observations and Data

We obtained MUSE observations in the field of PKS 0405−123 as part of the MUSE Quasar-field Blind Emitter Survey (MUSE-QuBES), a guaranteed time observation program (GTO) on the Very Large Telescope (VLT; PI: J. Schaye, PID: 094.A-0131). The MUSE-QuBES motivations, survey strategy, and analysis will be detailed in M. A. Segers et al. (in preparation) and L. A. Straka et al. (in preparation). The data are briefly summarized here.

MUSE is an IFS with a $1' \times 1'$ arcmin field of view (FOV), spectral coverage of 4750–9350 Å, and resolution of $R = 2000$–4000 (Bacon et al. 2010). We acquired 9.75 hr of MUSE integration for the field of PKS 0405−123 in 2014 October −November under median FWHM seeing of 0″.7 and reduced the data using GTO reduction (Weilbacher et al. 2014) and sky subtraction (Soto et al. 2016) tools. We identified continuum sources in the field with Source Extractor (Bertin & Arnouts 1996) using both a white-light image from the MUSE datacube and an image from the Advanced Camera (ACS) for Surveys aboard *Hubble Space Telescope* (*HST*) with the F814W filter (PI: J. S. Mulchaey, PID: 13024). For each source, we extracted a 1D spectrum using MPDAF (Piqueras et al. 2017) and measured initial redshifts with MARZ (Hinton et al. 2016). In the process, we discovered multiple extended nebulae at redshifts similar to the quasar that contaminate some redshift measurements. Consequently, we re-extracted the galaxy spectra with 0″.7 diameter apertures, masked strong emission lines, and measured the redshifts whenever possible based purely on stellar absorption by fitting Sloan Digital Sky Survey (SDSS) galaxy eigenspectra (Bolton et al. 2012). The resulting galaxy redshift uncertainties are ≈ 20 km s^{-1}.

The brightness of PKS 0405−123 and broad wings of the MUSE point-spread function (PSF) result in contribution of light from the quasar to spaxels at $\lesssim 8''$ from the quasar. However, PKS 0405−123 cannot be used to model the PSF because the host galaxy biases the model and stars in the field are not bright enough to measure the PSF wings.

To subtract the quasar light, we developed a technique that takes advantage of the spectral dimension provided by an IFS and the fact that galaxy and quasar spectra are distinct (see also Rupke et al. 2017). The primary challenge with this approach is the wavelength dependence of the PSF, which disperses blue light further away from the quasar than red light, resulting in an artificially flat (steep) quasar spectrum close to (far from) the quasar. To account for this, we determined the two non-negative spectral components that can best model the quasar contribution to any spaxel as linear combinations by performing non-negative matrix factorization (Zhu 2016) on quasar-dominated spaxels from a $1'' \times 1''$ aperture centered on the quasar. We then modeled each spaxel at $<8''$ from the quasar as a linear combination of the two quasar components and the first two SDSS galaxy eigenspectra shifted to $z = 0.57$ with emission lines masked. We subtracted the quasar component of the best-fit model from each spaxel, effectively removing the quasar light contribution except at $\lesssim 1''$ from the quasar.

3. The Galactic Environment of PKS 0405−123

We identified candidate members of the quasar host environment by selecting galaxies with line-of-sight (LOS) velocities of $|\Delta v| < 2000$ km s^{-1} from the quasar, $z_{QSO} = 0.5731 \pm 0.0003$ (measured from the [O II] line), including both our new MUSE catalog and galaxies outside the MUSE FOV from the ACS+F814W image with redshift measurements from the literature (see Johnson et al. 2013). We chose this velocity window to be approximately twice the velocity dispersion of the most massive galaxy clusters. We identified 31 (25) galaxies in the *HST* (MUSE) field within this velocity range, including the quasar host.

For each galaxy, we report the right ascension (R.A.), declination (decl.), observed ACS+F814W magnitude (m_{F814W}), redshift (z), rest-frame u–g color measured in matched isophotal apertures, rest-frame absolute r-band magnitude (M_r), and the projected angular ($\Delta\theta$), physical (d) and LOS velocity ($\Delta v = v - v_{QSO}$) differences from the quasar in Table 1. Figure 1 displays the ACS+F814W image of the field with group members labeled.

The quasar host environment includes 4 (20) galaxies of $M_r < -22$ (<-20), consistent with a massive galaxy group. The group velocity is $\Delta v = -460 \pm 150$ km s^{-1} from the quasar and the velocity dispersion is $\sigma_{group} = 430 \pm 140$ km s^{-1} based on galaxies of $M_r < -20$ as shown in the inset panel Figure 1 (with 2σ clipping and uncertainties from bootstrap resampling). Not including the quasar, the light-weighted group center is ≈ 8 pkpc west and ≈ 50 pkpc south of the quasar.

To gain insights into the environment of PKS 0405−123, we display a $30'' \times 30''$ cutout of the quasar-light–subtracted MUSE image averaged over 6000–7000 Å (free of strong emission lines at $z = 0.57$) in the top-left panel of Figure 2. The galaxy morphologies, projected separations, and relative velocities indicate that G6/G7, G9/G11, and G8/G10 are interacting galaxy pairs with projected separations of 34, 9, and 7 pkpc, respectively. G9/G11 are also nearly spatially coincident with one of the quasar radio lobes (see Sambruna et al. 2004), which is labeled with a blue triangle in Figure 2. All six of the interacting galaxies exhibit red rest-frame colors of u–$g = 1.1$–1.7.

G1/G2 are close projected pairs with one another (10 pkpc) and with the quasar (14 and 22 pkpc, respectively). The quasar-light–subtracted MUSE image shown in the top-left panel of

Table 1
Summary of Galaxies in the Field of PKS 0405−123 at $z \approx z_{\mathrm{QSO}}$

ID	R.A. (J2000)	Decl. (J2000)	m_{F814W} (AB)	z	$u-g$ (AB)	M_r (AB)	$\Delta\theta$ (arcsec)	d (pkpc)	Δv (km s^{-1})	Redshift Reference
Host	04:07:48.48	−12:11:36.0	⋯	0.5731	⋯	⋯	0.0	0.0	0	This work
G1	04:07:48.40	−12:11:34.2	21.3	0.5714	1.5	−21.3	2.2	14.3	−330	This work
G2	04:07:48.43	−12:11:32.8	21.7	0.5715	1.5	−20.9	3.3	21.9	−302	This work
G3	04:07:48.24	−12:11:42.2	23.6	0.5734	1.3	−19.0	7.1	46.5	+51	This work
G4	04:07:48.95	−12:11:37.7	22.8	0.5718	1.4	−19.8	7.1	46.8	−249	This work
G5	04:07:48.98	−12:11:38.8	23.8	0.5707	1.4	−18.8	7.9	51.4	−450	This work
G6	04:07:49.00	−12:11:31.8	21.1	0.5709	1.2	−21.3	8.8	57.3	−424	This work
G7	04:07:49.13	−12:11:36.7	21.9	0.5697	1.1	−20.5	9.7	63.2	−656	This work
G8	04:07:49.16	−12:11:42.7	20.7	0.5711	1.7	−21.7	12.0	78.6	−390	This work
G9	04:07:48.26	−12:11:47.8	20.0	0.5683	1.4	−22.3	12.2	79.9	−919	This work
G10	04:07:49.22	−12:11:42.0	21.5	0.5723	1.6	−20.9	12.5	81.7	−154	This work
G11	04:07:48.30	−12:11:49.2	20.9	0.5677	1.3	−21.4	13.4	87.7	−1025	This work
G12	04:07:48.66	−12:11:50.4	20.5	0.5656	1.7	−22.1	14.7	95.9	−1434	This work
G13	04:07:49.53	−12:11:39.3	22.3	0.5714	1.4	−20.3	15.8	103.4	−331	This work
G14	04:07:47.80	−12:11:49.3	22.8	0.5670	1.5	−19.5	16.6	108.4	−1165	This work
G15	04:07:48.76	−12:11:56.8	20.9	0.5710	1.8	−21.7	21.1	138.2	−395	This work
G16	04:07:49.78	−12:11:27.0	22.6	0.5709	1.6	−20.0	21.2	138.5	−415	This work
G17	04:07:47.72	−12:11:56.7	26.5	0.5742	0.8	−15.9	23.5	153.9	+206	This work
G18	04:07:49.89	−12:11:49.2	21.6	0.5691	1.7	−20.9	24.6	161.0	−763	This work
G19	04:07:48.53	−12:12:01.1	23.4	0.5742	1.5	−19.2	25.1	164.1	+200	This work
G20	04:07:47.47	−12:11:58.6	23.4	0.5642	1.6	−19.2	26.9	176.4	−1689	This work
G21	04:07:49.17	−12:12:02.4	20.7	0.5781	1.7	−22.0	28.3	185.1	+949	This work
G22	04:07:47.16	−12:12:01.3	22.8	0.5709	1.6	−19.8	31.8	208.3	−423	This work
G23	04:07:49.58	−12:12:04.8	25.5	0.5739	0.8	−16.9	33.0	216.2	+148	This work
G24	04:07:49.96	−12:11:09.5	21.8	0.5712	1.6	−20.8	34.3	224.8	−364	This work
G25	04:07:49.43	−12:12:10.8	21.0	0.5777	1.7	−21.6	37.5	245.4	+877	Ellingson et al. (1994)
G26	04:07:48.76	−12:12:18.6	21.4	0.5726	1.7	−21.1	42.8	279.9	−95	Johnson et al. (2013)
G27	04:07:46.63	−12:12:09.8	22.0	0.5725	1.4	−20.6	43.3	283.3	−114	Johnson et al. (2013)
G28	04:07:45.99	−12:10:59.8	20.1	0.5685	1.6	−22.3	51.5	336.9	−877	Chen & Mulchaey (2009)
G29	04:07:49.27	−12:12:26.3	22.8	0.5692	1.7	−19.6	51.5	337.4	−743	Johnson et al. (2013)
G30	04:07:46.50	−12:12:35.1	22.2	0.5675	0.7	−20.4	65.7	430.4	−1067	Johnson et al. (2013)

Figure 2 reveals an arm of continuum emission extending ≈60 pkpc to the north of the quasar, a signature of recent or ongoing interactions, possibly between the quasar host and G1/G2.

## 4. Discovery and Origins of 10–100 pkpc Scale Ionized Nebulae

The MUSE data enable the discovery of six ionized nebulae emitting strongly in [O III], [O II], and Hβ on scales of 10–100 pkpc and at LOS velocities of $\Delta v \approx -1000$ to $+200$ km s^{-1} from the quasar. To visualize the morphologies of these nebulae along with galaxies in the group, we display [O III] emission contours over the MUSE wideband image in the top-left panel of Figure 2. To visualize the kinematics of the nebulae and association with those of galaxies, the top-middle panel of Figure 2 displays a velocity map of the nebulae from Gaussian fitting. Subsequent panels display narrowband channels extracted from the datacube at the observed-frame wavelength of [O III] over velocities chosen to highlight each nebula and reveal detailed structure.

Here, we summarize the properties of the six nebulae and discuss their origins, proceeding from larger to smaller scales. Throughout, we refer to the nebulae by their position relative to the quasar as labeled in Figure 2: South (S.), East-by-South East (E.S.E), East (E.), South East (S.E.), Host South (H.S.), and Host North (H.N.). To quantify the properties of each

nebula, we measured the line luminosity in [O III], [O II], and Hβ, LOS velocity relative to the quasar (Δv), and LOS velocity dispersion (σ) by fitting Gaussian profiles to the emission lines at each spaxel with standard errors estimated from the MUSE error array and covariance matrix. We report the major axis position angle (PA); full extent along the major/minor axis; total line luminosity in [O III] (5008+4960), [O II] (3727 +3729), and Hβ; median Δv; median σ; and associated galaxies in Table 2. Uncertainties in emission line luminosities, velocities, and velocity dispersions are <15% and <20 km s^{-1}.

The nebulae exhibit high ionization states with mean [O III]/[O II] ratios of 1.3–3.5 (Figure 3), [O III]/Hβ of 4–10, and the brightest nebular regions exhibit He II λ4686 and [Ne V] λλ3346, 3426 detections. Such high ionization states can be produced by photoionization by the quasar (e.g., Groves et al. 2004) or fast shocks with velocities ≳400 km s^{-1} (e.g., Allen et al. 2008). The median internal velocity dispersions of the nebulae are low (50–130 km s^{-1}), which disfavors the shock scenario. Moreover, [O III]/[O II] ratios within each nebula are generally anti-correlated with the projected distance from the quasar (Figure 3), consistent with gas in the quasar host group that is photoionized by the quasar. In future work (S. D. Johnson et al. 2018, in preparation), we will present detailed studies of the physical conditions of the nebulae based on the full suite of available nebular diagnostics.

The three largest and most luminous nebulae (S., E.S.E., and E.) are kinematically and morphologically coincident with interacting
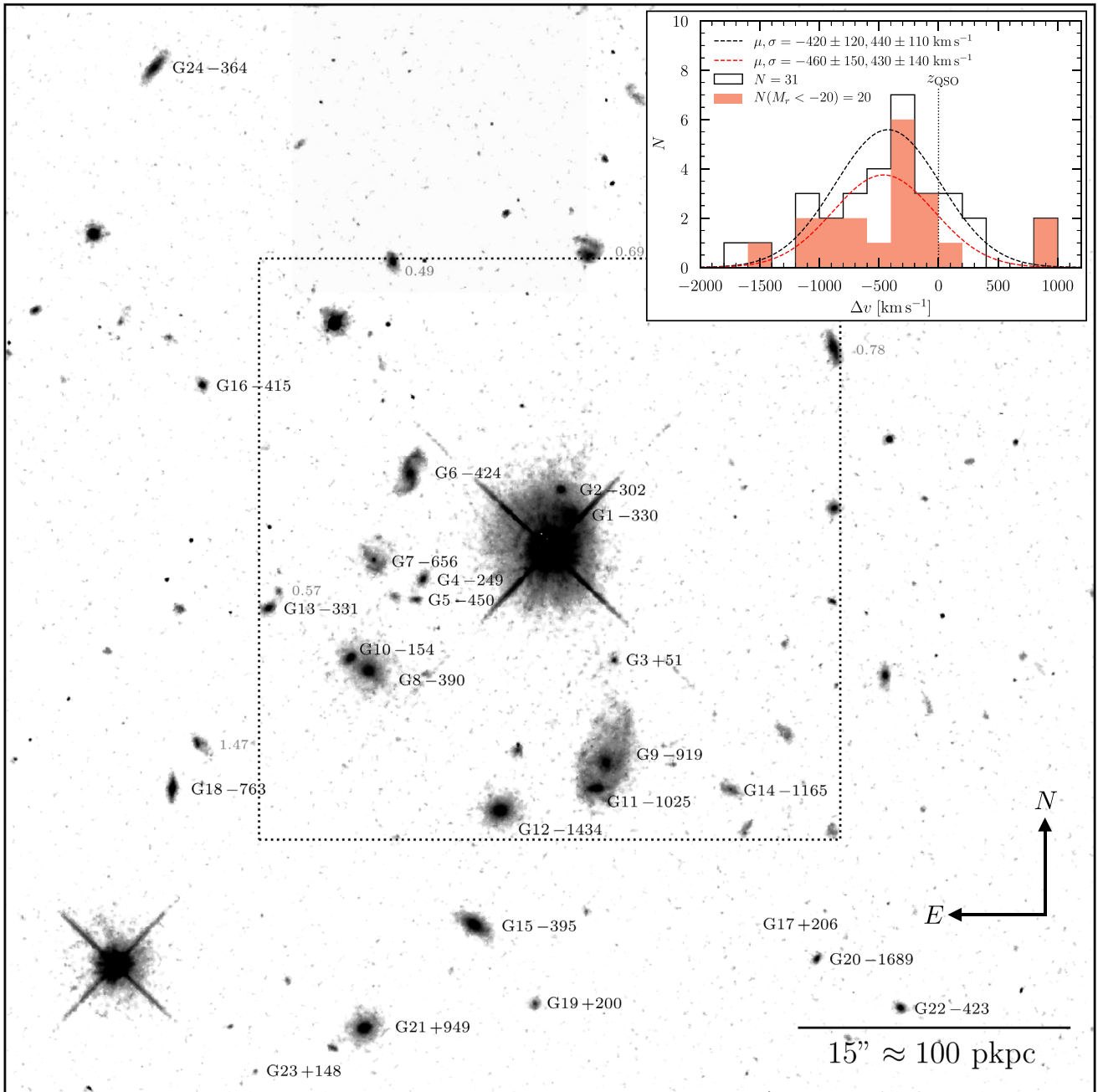
Figure 1. *HST* ACS/F814W image of the field of PKS 0405−123. Galaxies in the quasar host group are labeled by their ID and LOS velocity from the quasar ($z = 0.5731$) in km s^{-1}. Galaxies that are foreground (background) to the group are labeled in smaller font by their redshift from Johnson et al. (2013) in blue (gray). The image shows the $60'' \times 60''$ MUSE FOV and the dotted square marks the $30'' \times 30''$ region displayed in Figure 2. The inset panel displays the LOS velocity histogram of galaxies in the environment of PKS 0405−123, with the zero corresponding to the quasar systemic redshift.

galaxies in the field as shown in Figure 2. In particular, S., E.S.E, and E. spatially and kinematically envelope interacting galaxy pairs G9/G11, G8/G10, and G6/G7, respectively. The morphological and kinematic correspondence with interacting galaxies and the narrow internal velocity dispersions ($\sigma = 70$–110 km s^{-1}) are most consistent with stripped ISM resulting from ongoing interactions, despite the spatial coincidence between the S. nebulae and a radio lobe (see Harrison et al. 2015).

Unlike the other nebulae, S.E. is a narrow filament extending from $d \approx 55$ to 120 pkpc toward the quasar with a width of ≈ 10 pkpc (bottom-middle panel of Figure 2). S.E. is the faintest, lowest surface brightness, and most highly ionized of the nebulae despite being furthest from the quasar, suggesting that it has lower density. S.E. exhibits a median velocity $\Delta v = -140$ km s^{-1} and a narrow median velocity dispersion of 50 km s^{-1}. S.E. is not associated with any nearby galaxies detected in the *HST* or MUSE images, which are complete for $m_{\mathrm{F814W}} \lesssim 26.5$ mag sources ($M_r = -16$ at $z = 0.57$). The morphology, calm kinematics, low surface brightness, high ionization state, and lack of any associated galaxies all suggest that S.E. is a cool filament in the IGrM.

H.N. and H.S. are spatially and kinematically coincident with the quasar host at $d \approx 10$ pkpc to the north and south and

4
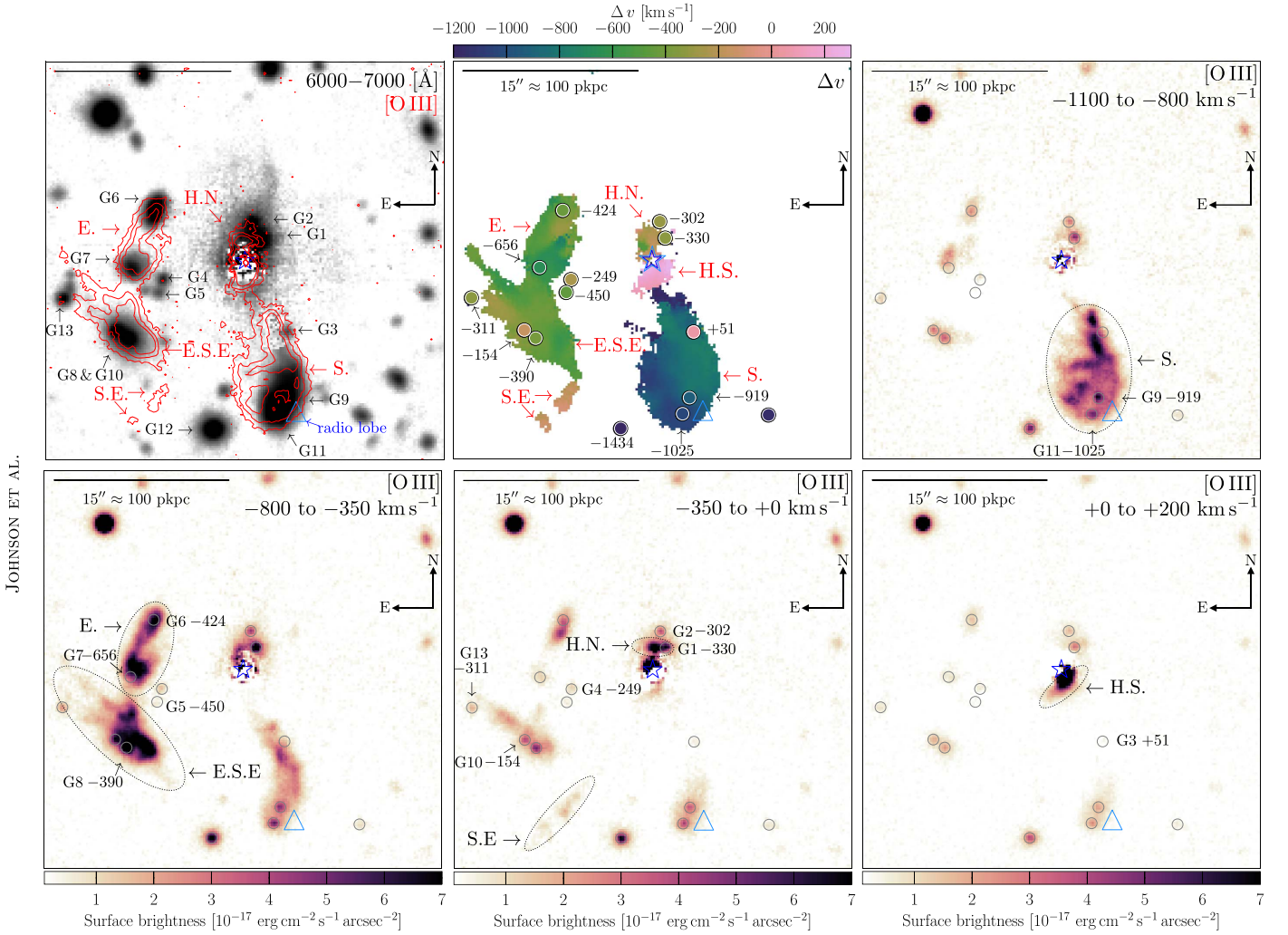
Figure 2. Top-left panel: median flux over 6000–7000 Å in the MUSE datacube with [O III] surface brightness contours of 0.75, 2.5, and 5 × 10^{-17} erg cm^{-2} s^{-1} arcsec^{-2} in red and with galaxies and nebulae labeled. Top-middle panel: map of the nebular LOS velocities relative to the quasar. The positions of galaxies in the host group are marked by circles with LOS velocity on the same scale. The top-right panel and bottom row show narrowband [O III] images extracted from the MUSE datacube over LOS velocity intervals indicated in each panel. Nebulae are marked by ellipses and labeled, while the quasar and radio lobe are marked by a blue star and triangle, respectively. Galaxies are labeled if they fall within the displayed velocity interval.

with median velocities of $\Delta v = -230$ and $+150$ km s^{-1}, respectively. They extend over $\approx$20–30 pkpc and are morphologically reminiscent of tidal arms (bottom-middle and right panels of Figure 2). H.N. and H.S. and the extended arm of continuum emission seen north of the host may be the result of ongoing interactions with G1/G2 or another more advanced merger. The H.N. and H.S. nebulae exhibit similar [O III] to [O II] ratios to the other nebulae, despite being significantly closer to the quasar. This is consistent with expectations for the ISM of the quasar host, which is likely to have higher densities than either stripped ISM or cool filaments. We do not detect any nebular emission associated with the continuum arm. Adopting the measured velocities and projected distances of H.N. and H.S., we estimate a dynamical mass for the quasar host of $M_{\rm dyn}(<10\,{\rm pkpc}) \sim 10^{11}\,M_\odot/\sin^2 i$ where i is the inclination angle (assuming $v^2(r) \approx GM(<r)/r$).

5. Discussion and Conclusions

With deep MUSE observations, we discovered six ionized nebulae on scales of 10–100 pkpc in the $z \approx 0.57$ galaxy group hosting PKS 0405−123, one of the most luminous quasars at

$z < 1$. Although the nebulae are distributed over a wide range of PAs and projected distances from the quasar, all exhibit line ratios that are most consistent with quasar photoionization, requiring a large opening angle and an active lifetime of $\gtrsim 3 \times 10^5$ yr (the light travel time for $\approx$100 kpc). The quasar photoionization enables observations of cool IGrM and ISM that would otherwise be neutral and not observable in emission beyond the local Universe. When combined with the morpho-kinematic information from a wide-field IFS, this enables new insights into galaxy and quasar fuel supplies from the IGrM to the ISM.

One of the nebulae (S.E.) exhibits a filamentary morphology extending 50 pkpc toward the quasar with narrow internal velocity dispersion (50 km s^{-1}) and is not associated with any detected galaxies. These properties are most consistent with a cool filament in the IGrM like those observed more locally in groups (e.g., Xu et al. 1999) and in cool-core clusters (e.g., McDonald et al. 2010; Gaspari et al. 2018). Such filaments often occur in central networks, but are also observed in what would appear as single filaments in our seeing limited data (e.g., Abell 1796). The truncation of the filamentary nebulae before reaching the quasar host would be unusual in a cluster,

Table 2
Summary of the Properties of the Ionized Nebulae

Nebula	PA (deg.)	Major Axis (pkpc)	Minor Axis (pkpc)	Area (pkpc²)	Total Line Luminosity			Median		Associated Galaxies
					[O III] (erg s⁻¹)	[O II] (erg s⁻¹)	Hβ (erg s⁻¹)	Δv (km s⁻¹)	σ (km s⁻¹)	
H.N.	355	24	10	190	2.8×10^{41}	8.3×10^{40}	6.7×10^{40}	−230	130	host, G1, G2
H.S.	40	34	10	280	7.6×10^{41}	2.4×10^{41}	9.0×10^{40}	+150	100	host, G1, G2
S.	92	72	48	2440	3.4×10^{42}	1.3×10^{42}	5.6×10^{41}	−900	70	G9, G11
S.E.	47	56	13	480	9.2×10^{40}	2.6×10^{40}	8.8×10^{39}	−140	50	none
E.S.E.	317	96	33	2340	2.1×10^{42}	1.0×10^{41}	2.4×10^{41}	−420	90	G8, G10
E.	73	54	29	1430	1.6×10^{42}	1.2×10^{42}	2.7×10^{41}	−500	110	G6, G7
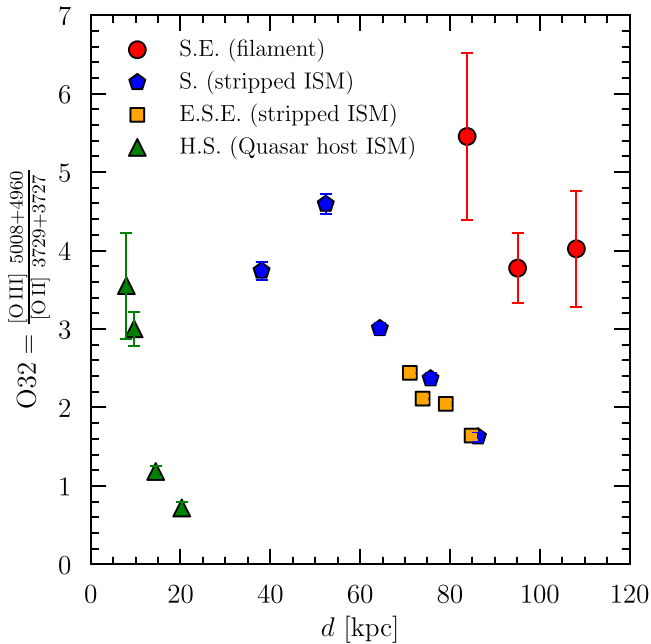
Figure 3. [O III] 5008+4960 to [O II] 3729+3727 emission line ratio as a function of projected distance from the quasar for the S.E., S., E.S.E., and H.S. nebulae as indicated in the figure legend. The H.N. and E. nebulae are not shown because they offer little leverage in projected distance.

but may result from increased ionization state at smaller distances from the quasar weakening optical emission lines.

The superb imaging and spectral quality of MUSE enable the subtraction of the quasar light to reveal a 60 kpc arm of continuum emission and two ≈10 pkpc tidal-arm–like nebulae extending from the quasar host, all signatures of interactions. The presence of a cool filament extending toward the host, continuum arm, and nebulae near the host make PKS 0405 −123 one of the strongest candidates for an interaction-triggered quasar and an ideal case study of the relationship between galaxy/black hole growth and gas supplies on scales from the IGrM (≈100 pkpc) to the ISM (≈10 pkpc). In particular, the filamentary nebula (S.E.) may have supplied the ISM of the quasar host with cooling IGrM, while interactions may redistribute angular momentum in ISM to fuel nuclear activity.

The three largest nebulae (S., E.S.E, and E.) are among the largest and most luminous [O III] "blobs" known (e.g., Schirmer et al. 2016; Yuma et al. 2017; Epinat et al. 2018). They exhibit large LOS velocities relative to the quasar (−900 to −400 km s⁻¹) but narrow internal velocity dispersions (70–110 km s⁻¹). Joint morphological and kinematic analyses

indicate that these three nebulae originate from ISM stripped from interacting galaxies in the host group rather than from outflows, as is often assumed (e.g., Fu & Stockton 2009; Yuma et al. 2017). The stripping may be due to tidal forces (e.g., Marasco et al. 2016) or ram pressure (e.g., Hester 2006), which can remove H I disks and decrease star formation in even massive satellites that interact with one another or pass through central, dense IGrM regions. The velocity shear, one-sided morphology and sharp truncation of the S. nebulae are suggestive of ram pressure stripping though variability, or partial obscuration of the quasar may also be responsible. Such large nebulae from stripped material could potentially explain the densest components of extended nebulae observed around luminous quasars at $z > 2$ (e.g., Borisova et al. 2016; Law et al. 2018).

The discovery of extended, ionized nebulae including a cool filament and interaction-related debris in the environment of PKS 0405−123 demonstrate the power of wide-field IFS for studying quasar hosts. The nebulae cover 20% of the area around the quasar at ≲100 kpc, which may explain the high covering fraction of absorbing gas around luminous quasar hosts (Johnson et al. 2015) if the gas extends to larger distances at lower densities. In future work (S. D. Johnson et al., in preparation), we will present a survey of the ionized nebulae around quasar hosts from the full MUSE-QuBES sample including the full suite of available nebular diagnostic.

ORCID iDs

Sean D. Johnson ⓘ https://orcid.org/0000-0001-9487-8583
Hsiao-Wen Chen ⓘ https://orcid.org/0000-0001-8813-4182
Lorrie A. Straka ⓘ https://orcid.org/0000-0001-5892-6760
Joop Schaye ⓘ https://orcid.org/0000-0002-0668-5560
Sowgat Muzahid ⓘ https://orcid.org/0000-0003-3938-8762
Nicolas Bouché ⓘ https://orcid.org/0000-0003-0068-9920
Raffaella A. Marino ⓘ https://orcid.org/0000-0002-8559-6565
Michael V. Maseda ⓘ https://orcid.org/0000-0003-0695-4414

References

Allen, M. G., Groves, B. A., Dopita, M. A., Sutherland, R. S., & Kewley, L. J. 2008, ApJS, 178, 20

Bacon, R., Accardo, M., Adjali, L., et al. 2010, Proc. SPIE, 7735, 773508

Berg, T. A. M., Ellison, S. L., Tumlinson, J., et al. 2018, arXiv:1805.05348

Bertin, E., & Arnouts, S. 1996, A&AS, 117, 393

Bolton, A. S., Schlegel, D. J., Aubourg, É., et al. 2012, AJ, 144, 144

Borisova, E., Cantalupo, S., Lilly, S. J., et al. 2016, ApJ, 831, 39

Bowen, D. V., Hennawi, J. F., Ménard, B., et al. 2006, ApJL, 645, L105

Chen, H.-W., & Mulchaey, J. S. 2009, ApJ, 701, 1219

Chen, H.-W., Zahedy, F. S., Johnson, S. D., et al. 2018, MNRAS, 479, 2547

Ellingson, E., Yee, H. K. C., Bechtold, J., & Dobrzycki, A. 1994, AJ, 107, 1219

Epinat, B., Contini, T., Finley, H., et al. 2018, A&A, 609, A40

Farina, E. P., Falomo, R., Scarpa, R., et al. 2014, MNRAS, 441, 886

Fu, H., & Stockton, A. 2009, ApJ, 690, 953

Gaspari, M., McDonald, M., Hamer, S. L., et al. 2018, ApJ, 854, 167

Goulding, A. D., Greene, J. E., Bezanson, R., et al. 2018, PASJ, 70, S37

Greene, J. E., Zakamska, N. L., & Smith, P. S. 2012, ApJ, 746, 86

Groves, B. A., Dopita, M. A., & Sutherland, R. S. 2004, ApJS, 153, 75

Harrison, C. M., Thomson, A. P., Alexander, D. M., et al. 2015, ApJ, 800, 45

Hennawi, J. F., Strauss, M. A., Oguri, M., et al. 2006, AJ, 131, 1

Hester, J. A. 2006, ApJ, 647, 910

Hinton, S. R., Davis, T. M., Lidman, C., Glazebrook, K., & Lewis, G. F. 2016, A&C, 15, 61

Hopkins, P. F., & Hernquist, L. 2009, ApJ, 694, 599

Husemann, B., Wisotzki, L., Sánchez, S. F., & Jahnke, K. 2013, A&A, 549, A43

Johnson, S. D., Chen, H.-W., & Mulchaey, J. S. 2013, MNRAS, 434, 1765

Johnson, S. D., Chen, H.-W., & Mulchaey, J. S. 2015, MNRAS, 452, 2553

Law, D. R., Steidel, C. C., Chen, Y., et al. 2018, arXiv:1809.04089

Liu, G., Zakamska, N. L., Greene, J. E., Nesvadba, N. P. H., & Liu, X. 2013, MNRAS, 436, 2576

Marasco, A., Crain, R. A., Schaye, J., et al. 2016, MNRAS, 461, 2630

McAlpine, S., Bower, R. G., Rosario, D. J., et al. 2018, arXiv:1805.08293

McDonald, M., Veilleux, S., Rupke, D. S. N., & Mushotzky, R. 2010, ApJ, 721, 1262

Piqueras, L., Conseil, S., Shepherd, M., et al. 2017, arXiv:1710.03554

Poggianti, B. M., Jaffé, Y. L., Moretti, A., et al. 2017, Natur, 548, 304

Powell, M. C., Husemann, B., Tremblay, G. R., et al. 2018, arXiv:1807.00839

Prochaska, J. X., Hennawi, J. F., Lee, K.-G., et al. 2013, ApJ, 776, 136

Punsly, B., Marziani, P., Zhang, S., Muzahid, S., & O'Dea, C. P. 2016, ApJ, 830, 104

Robitaille, T., & Bressert, E. 2012, APLpy: Astronomical Plotting Library in Python, Astrophysics Source Code Library, ascl:1208.017

Rupke, D. S. N., Gültekin, K., & Veilleux, S. 2017, ApJ, 850, 40

Sambruna, R. M., Gambill, J. K., Maraschi, L., et al. 2004, ApJ, 608, 698

Schirmer, M., Malhotra, S., Levenson, N. A., et al. 2016, MNRAS, 463, 1554

Schmidt, M., Schneider, D. P., & Gunn, J. E. 1995, AJ, 110, 68

Soto, K. T., Lilly, S. J., Bacon, R., Richard, J., & Conseil, S. 2016, ZAP: Zurich Atmosphere Purge, Astrophysics Source Code Library, ascl:1602.003

Stockton, A., & MacKenty, J. W. 1987, ApJ, 316, 584

Sun, A.-L., Greene, J. E., & Zakamska, N. L. 2017, ApJ, 835, 222

The Astropy Collaboration, Price-Whelan, A. M., Sipőcz, B. M., et al. 2018, arXiv:1801.02634

Villar-Martín, M., Tadhunter, C., Pérez, E., et al. 2010, MNRAS, 407, L6

Villforth, C., Hamann, F., Rosario, D. J., et al. 2014, MNRAS, 439, 3342

Weilbacher, P. M., Streicher, O., Urrutia, T., et al. 2014, in ASP Conf. Ser. 485, Astronomical Data Analysis Software and Systems XXIII, ed. N. Manset & P. Forshay (San Francisco, CA: ASP), 451

Xu, C., Sulentic, J. W., & Tuffs, R. 1999, ApJ, 512, 178

Yuma, S., Ouchi, M., Drake, A. B., et al. 2017, ApJ, 841, 93

Zhu, G. 2016, arXiv:1612.06037